Title

Preliminary Assignment of Protonated and Deprotonated Homocitrates in Extracted FeMo-Cofactors by Comparisons with Molybdenum(IV) Lactates and Oxidovanadium Glycolates

Journal

Inorganic Chemistry, 58(4)

ISSN

0020-1669

Authors

Jin, Wan-Ting
Wang, Hongxin
Wang, Si-Yuan
et al.

Publication Date

2019-02-18

DOI

10.1021/acs.inorgchem.8b03108

Peer reviewed

HHS Public Access

Author manuscript

Inorg Chem. Author manuscript; available in PMC 2019 October 25.

Published in final edited form as:

Inorg Chem. 2019 February 18; 58(4): 2523–2532. doi:10.1021/acs.inorgchem.8b03108.

Preliminary Assignment of Protonated and Deprotonated Homocitrates in Extracted FeMo-cofactors by Comparisons with Molybdenum(IV) Lactates and Oxidovanadium Glycolates

Wan-Ting Jin[a], **Hongxin Wang**[b,c], **Si-Yuan Wang**[a], **Christie H. Dapper**[d], **Xing Li**[a], **William E. Newton**[d], **Zhao-Hui Zhou**[*,a], **Stephen P. Cramer**[*,b,c]

[a]State Key Laboratory of Physical Chemistry of Solid Surfaces, College of Chemistry and Chemical Engineering, Xiamen University, Xiamen, 361005, China.

[b]Department of Chemistry, University of California, Davis, CA 95616.

[c]Physical Biosciences Division, Lawrence Berkeley National Laboratory, Berkeley, CA, 94720.

[d]Department of Biochemistry, Virginia Polytechnic Institute & State University, Blacksburg, VA 24061

Abstract

A similar pair of protonated and deprotonated mononuclear oxidovanadium glycolates $[VO(Hglyc)(phen)(H_2O)]Cl{\cdot}2H_2O$ (**1**) and $[VO(glyc)(bpy)(H_2O)]$ (**2**) and a mixed-(de)protonated oxidovanadium triglycolate $(NH_4)_2[VO(Hglyc)_2(glyc)]{\cdot}H_2O$ (**3**) were isolated and examined. The ≡C–O(H) (≡C–OH or ≡C–O) groups coordinated to vanadium were spectroscopically and structurally identified. The glycolate in **1** features a bidentate chelation through protonated α-hydroxy and α-carboxy groups, whereas the glycolate in **2** coordinates through deprotonated α-alkoxy and α-carboxy groups. The glycolates in **3** coordinate to vanadium through α-alkoxy or α-hydroxy and α-carboxy groups, and thus has both protonated ≡C–OH and deprotonated ≡C–O bonds simultaneously. Structural investigations revealed that the longer protonated $V–O_{\alpha\text{-hydroxy}}$ bonds [2.234(2) Å and 2.244(2) Å] in **1** and **3** are close to those of FeV-co 2.17 Å[1] (FeMo-co 2.17 Å[2]), while deprotonated $V–O_{\alpha\text{-alkoxy}}$ bonds [**2**, 1.930(2); **3**, 1.927(2) Å] were obviously shorter. This shows a similar elongated trend as the Mo–O distances in the previously reported deprotonated *vs.* protonated molybdenum lactates,[3] and these vanadium and molybdenum complexes have the same local V/Mo-homocitrate structures as those of FeV/Mo-cos of nitrogenases. The IR spectra of these oxidovanadium and the previously synthesized molybdenum complexes including different substituted ≡C–O(H) model compounds show red-shifts for ≡C–OH

[*]**Corresponding Authors:** Zhao-Hui Zhou. zhzhou@xmu.edu.cn; Fax: +86 592 2183047; Tel: +86 592 2184531., Stephen P. Cramer. spjcramer@ucdavis.edu; Tel: (530) 752-0360.

ASSOCIATED CONTENT

Supporting Information

CCDC 1472398, 1472399 and 1570694 contain the supplementary crystallographic data for **1** ~ **3**. The Supporting Information is available free of charge *via* the Internet at http://pubs.acs.org. It contains three parts of information: **Part I** Syntheses of $[VO(phen)_2Cl]Cl{\cdot}H_2O$[77] and $[VO_2(bpy)_2]Cl{\cdot}4H_2O$[78], ORTEP plots, packing diagrams, UV-Vis, FT-IR, EPR, Crystallographic data, selected bond distances and angles, hydrogen bonds, valence bond analyses for complexes **1** ~ **3**. The comparisons of V/Mo–O distances in α-hydroxycarboxylato vanadium/molybdenum complexes. **Part II** FT-IR spectrum of extracted FeMo-co. **Part III** IR spectra of all the compounds in Tables 2 and 3.

Wang-Tin Jin and Hongxin Wang are co-first authors. The authors declare no competing financial interest.

vs. ≡C–O alternation, which further assign the two IR bands of extracted FeMo-co at 1084 and 1031 cm^{-1} to ≡C–O and ≡C–OH vibrations respectively. Although the structural data or IR spectra for some of the previously synthesized Mo/V complexes and extracted FeMo-co were measured earlier, this is the first time that the ≡C–O(H) coordinated peaks are assigned. The overall structural and IR results well suggest the co-existence of homocitrates coordinated with α-alkoxy (deprotonated) and α-hydroxy (protonated) groups in the extracted FeMo-co.

Graphical Abstract

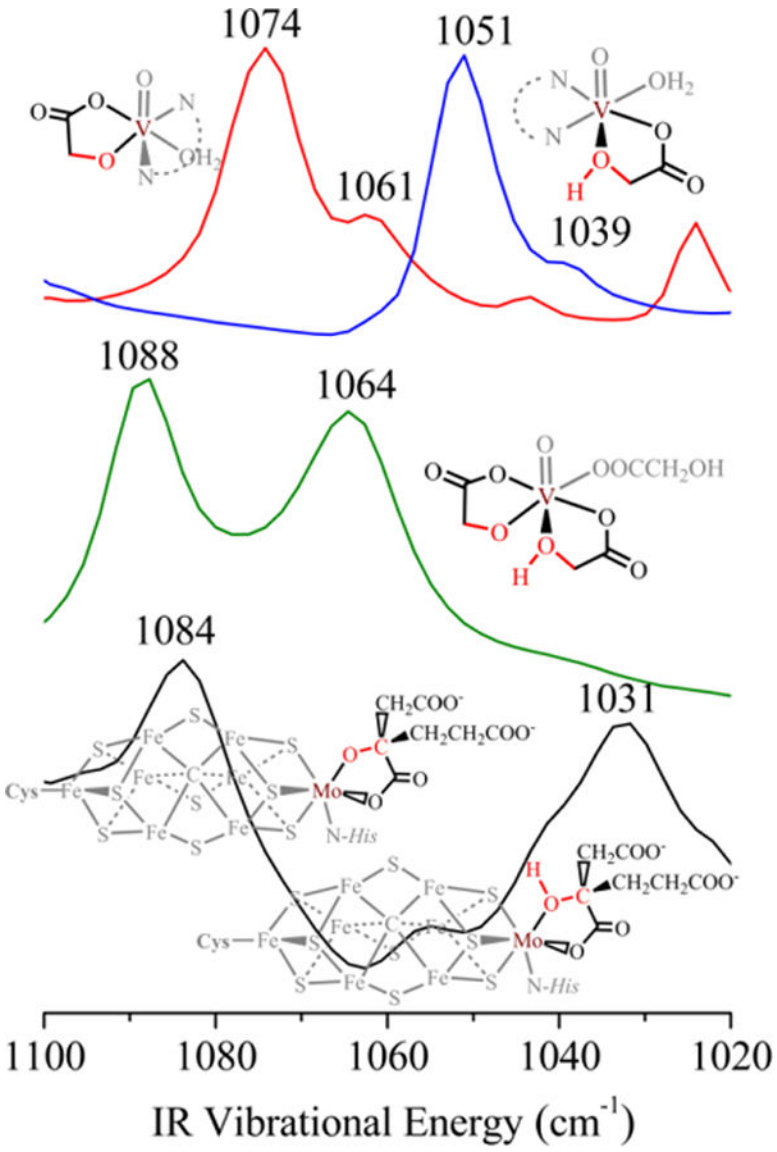

A similar pair of protonated and deprotonated mononuclear oxidovanadium glycolates $[VO(Hglyc)(phen)(H_2O)]Cl{\cdot}2H_2O$ (**1**) and $[VO(glyc)(bpy)(H_2O)]$ (**2**) and a mixed-(de)protonated oxidovanadium triglycolate $(NH_4)_2[VO(Hglyc)_2(glyc)]{\cdot}H_2O$ (**3**) were isolated. The structural comparison and IR spectra of these oxidovanadium complexes as well as the previously synthesized molybdenum complexes are cited for the IR assignment of ≡C–O(H) vibrations in

extracted FeMo-cofactor, suggesting co-existence of homocitrates coordinated with α-alkoxy (deprotonated) and α-hydroxy (protonated) groups in the extracted FeMo-co.

Keywords

Infrared spectroscopy; hydroxycarboxylate; FeMo-cofactor; FeV-cofactor; nitrogenase

INTRODUCTION

Nitrogenases catalyze the reduction of dinitrogen (N_2) to ammonia (NH_3) in nature. The enzymes have been extensively investigated and the structures of their catalytic active sites FeMo/V-cofactors (FeMo/V-cos) have been finally clarified as $MoFe_7S_9C$(cys)(Hhis)(*R*-homocit)[2,4–6] and VFe_7S_8C(cys)(Hhis) (XO_3)(*R*-homocit) (H_4homocit = homocitric acid, X = C or N respectively, Hcys = cysteine, $C_3H_7NO_2S$, Hhis = histidine, $C_6H_9N_3O_2$),[1,7] where homocitrates coordinate with metal Mo or V *via* the oxygen atoms of α-alkoxy and α-carboxy groups and have a charge of −4.[8] Spectroscopic studies with infrared spectroscopy (IR),[9,10] magnetic-circular-dichroism spectroscopy (MCD),[11,12] ^{19}F nuclear magnetic resonance spectroscopy (^{19}F NMR),[13] X-ray absorption spectroscopy (XAS),[14–19] Mössbauer spectroscopy,[20,21] electron-nuclear double resonance (ENDOR),[22,23] electron spin echo envelope modulation (ESEEM),[22,23] impulsive coherent vibrational spectroscopy (ICVS),[24] nuclear resonance vibrational spectroscopy (NRVS),[25,26] and electron paramagnetic resonance (EPR)[20,27] show a low valence and paramagnetic nature for FeMo/V-cos. The charge on FeMo-co has been controversial as the metal oxidation states of FeMo-co were suggested as Mo(IV)6Fe(II)1Fe(III),[28] Mo(IV)4Fe(II)3Fe(III),[29] Mo(IV)2Fe(II)5Fe(III)[30] and Mo(III)3Fe(II)4Fe(III) respectively.[31,32] In addition to the FeMo/V-cos' central structures, the local structure about the Mo/V-homocitrato coordination is critical for the nitrogenase studies. We have suggested a protonated model for FeMo/V-cos based on a computational study[33] and protonated α-hydroxycarboxylato oxidovanadium complexes.[34] Structural comparisons of glycolato and lactato molybdenum(IV) complexes and nitrogenases provide indirect evidence for the protonation of homocitrate in FeMo-co.[3] In addition, there are several recent theoretical computational calculations for the favorite protonation states in α-alkoxy group of homocitrate ligand of FeMo-co.[30,35–37]

Most of the previous glycolate, lactate, malate, citrate or homocitrate bind to vanadium or molybdenum *via* α-alkoxy and α-carboxy, and/or β-carboxy groups,[38–63] while only a small number of complexes were isolated coordinating *via* α-hydroxy (protonated) and α-carboxy groups.[34,64–68] As the homocitrates in the cofactors have a bidentate coordination, protonated and deprotonated molybdenum/vanadium α-hydroxycarboxylates with the similar local structures are critical for comparisons with the FeMo/V-cos and for a better clarification of their coordination environments. In this publication, we report the successfully isolated protonated and deprotonated pair of mononuclear glycolato oxidovanadium complexes: $[VO(Hglyc)(phen)(H_2O)]Cl{\cdot}2H_2O$ (**1**), $[VO(glyc)(bpy)(H_2O)]$ (**2**) (H_2glyc = glycolic acid, bpy = 2,2'-bipyridine, phen = 1,10-phenanthroline). Oxidovanadium triglycolate $(NH_4)_2[VO(Hglyc)_2(glyc)]{\cdot}H_2O$ (**3**) with a mixed-(de)protonated state was also synthesized and analyzed. All these complexes have a similar

bidentate chelated local structure as the homocitrate has in FeV-co or FeMo-co. The infrared spectrum (IR) of the extracted FeMo-co[9,69,70] has been re-examined. The structures and IR spectra of the above vanadium complexes (**1** ~ **3**) are compared with those of FeMo/V-cos, as well as compared with the protonated and deprotonated molybdenum(IV) lactates $[Mo^{IV}_3S_4(PPh_3)_3(Hlact)_2(lact)]$,[62] $Na_2[Mo^{IV}_3SO_3(R,S\text{-lact})_3(im)_3]\cdot 10H_2O$[3,67] and different substituted ≡C–O(H) model compounds. Although the structural data or IR spectra for some of the previously synthesized Mo/V complexes were measured earlier, this is the first time that the ≡C–O(H) coordinated peaks are assigned. *Via* these comparisons, the protonated/deprotonated states of homocitrate in extracted FeMo-co are assigned experimentally and discussed systematically for the first time.

RESULTS AND DISCUSSION

Syntheses.

In the preparations of **1** and **2**, the precursor V_2O_5 was reduced to VO^{2+} species by water in acidic solution under hydrothermal condition. The reactions of V_2O_5 with excess glycolic acid and N-chelated ligands are sensitive to the pH values. The deprotonated **2** was isolated at pH 3.0 in the presence of bipyridine, while the protonated **1** was obtained under low pH value of 1.0 in the presence of phenanthroline. The reactant of bipyridine or phenanthroline was not in excess. **3** was obtained from the reaction of $VOSO_4$ with three equivalents of glycolic acid without the participation of N-chelated ligand.[24,25] The synthesis of **3** was at room temperature but the crystallization was found sensitive to the temperature and the concentration of the reactants. Moreover, the effects of pH variations between 4 ~ 6 and the ratio of V:ligand (1:2 or 1:3) seem less crucial for the formation of **3** in comparison with the cases in **1** and **2**. The complexes **1** and **3** are soluble in water, while **2** is insoluble.

Crystal Structures.

The ORTEP diagrams of **1** ~ **3** are shown in the Supplementary Information (SI†) - Figs. S1 ~ S3. The detailed X-ray crystallographic data and the selected bond distances and angles for **1** ~ **3** are listed as in Tables S1 ~ S3. X-ray crystallographic analyses reveal that the glycolate in **1** coordinates bidentately to vanadium atom *via* protonated α-hydroxy and α-carboxy groups, while the glycolate in neutral molecule **2** coordinates *via* deprotonated α-alkoxy and α-carboxy groups. The V(IV) ions in **1** and **2** exist in distorted octahedral geometries with N_2O_4 donor set. In **1**, two nitrogen atoms of phenanthroline (N1 and N2) and one oxygen atom of water molecule (O1w), as well as the oxygen atom in α-carboxy group of glycolate (O2) occupy the four equatorial positions. The oxygen atom in α-hydroxy group of glycolate (O1) is at one axial position, *trans* to the terminal oxygen atom (O4) on the other axial site. The 2-D packing diagram of **1** is provided in Fig. S4, showing hydrophobic π–π interaction of phenanthroline. In **2**, the oxygen atoms in α-alkoxy (O1) and α-carboxy groups (O2) are at two equatorial positions, while one coordinated water molecule (O1w) and one nitrogen atom of bpy (N1) occupy the other two equatorial positions. The other nitrogen atom of bpy (N2) is at one axial position and the terminal oxygen atom (O4) is at the final axial site. The 2-D packing diagram of **2** is given in Fig. S5, showing hydrophobic π–π interaction of bipyridine.

The vanadium ion in **3** coordinates with three glycolates, presenting a distorted octahedral geometry. One of the glycolates coordinates *via* α-alkoxy (O3) and α-carboxy (O4) groups, where the two oxygen atoms are at two equatorial positions. The second glycolate coordinates to vanadium *via* α-carboxy group (O5), leaving the α-hydroxy group (O10) free. The last glycolate coordinates *via* α-hydroxy (O1) and α-carboxy (O2) groups, where the α-hydroxy (O1) is *trans* to terminal oxygen atom (O6) on the final axial site. Coordinating with both of the protonated and deprotonated glycolates, **3** can serve as a mixed-(de)protonated model complex compared with **1** and **2**. The anion structure of **3** is similar to the reported potassium salt $K_2[VO(Hglyc)_2(glyc)]\cdot H_2O$.[64,65]

The structural environments near the V-glycolate coordinations of **1** ~ **3** are shown in Fig. 1, and their hydrogen bonds are listed in Table S3. For **1**, α-hydroxy group forms strong hydrogen bond with α-carboxy group [O1···O3a 2.71(1) Å, *a* (*x* + ½, -*y* + ½, *z* + ½)], and the coordinated water molecule forms strong hydrogen bonds with crystal water molecules [O1wa···O2wa 2.62(1) Å; O1wa···O3wa 2.58(1) Å]. The free chloride anions also connect with the lattice water molecules by hydrogen bonds [Cl1a···O3wa 3.03(1) Å; Cl1a···O2wb 3.05(1) Å, *b* (*x* + ½, -*y* + ½, *z* + 3/2); and Cl1a···O3wc 3.15(1) Å, *c* (*x* + ½, *y* - ½, *z* + 1)]. For **2**, the coordinated water molecules form strong hydrogen bonds with α-alkoxy and α-carboxy groups [O1w···O1a 2.58(1) Å, *a* (-*x* + 1, -*y*, -*z* + 2); O1w···O3b 2.65(1) Å, *b* (-*x* + 1, *y* − ½, -*z* + 3/2)]. For **3**, a mixed-(de)protonated state is formed in **3** as the strong interactions of hydrogen bonds are favourable for the proton exchange between α-alkoxy and α-hydroxy groups. The α-alkoxy O3 and α-hydroxy O1 form strong hydrogen bonds with α-hydroxy O1a and α-alkoxy O3a from the adjacent molecule respectively. The distance of hydrogen bond [O1···O3a 2.55(1) Å, *a* (1 − *x*, 1 − *y*, 1 − *z*)] is similar to the O···O distance (2.50 Å) calculated by a protonated QM/MM model.[35]

The V−O distances of α-hydroxycarboxylato vanadium complexes vary systematically according to the bond types and the oxidation states of the vanadium ions. Theoretical bond valence calculations[71,72] (Table S4) and EPR spectra (Figure S6) gave the valence of +4 for **1** ~ **3** respectively. As shown in Table 1, protonated and deprotonated oxidovanadium products **1** and **2** exhibit different V–O distances. The $V1–O1_{\alpha\text{-hydroxy}}$ distance in **1** [2.231(2) Å] (protonated) is much longer than that of $V1–O1_{\alpha\text{-alkoxy}}$ in **2** [1.931(2) Å] (deprotonated). In **3**, the $V1–O1_{\alpha\text{-hydroxy}}$ distance [2.244(2) Å] (protonated) is found longer than $V1–O3_{\alpha\text{-alkoxy}}$ distance [1.927(2) Å] (deprotonated). The difference (~ 0.3 Å) between $V–O_{\alpha\text{-hydroxy}}$ and $V–O_{\alpha\text{-alkoxy}}$ distances can be attributed to the *trans* effect of V=O group and the equalization of electronic cloud density resulted from the protonation. The protonation contributes about 0.1 Å to the change of $V–O_{\alpha\text{-hydroxy}}$ distance when excluding the *trans* effect from V=O group, which is supported by the protonated complexes $[VO(C_5H_9O_3)_2(C_5H_8N_2)]$[67] [V1–O2 (protonated, axial site), 2.209(2) Å; V1–O5 (protonated, equatorial site), 2.023(2) Å] and $[VO(H_2cit)(phen)]_2\cdot 6.5H_2O$ [V1–O1 (protonated, axial site), 2.203(5) Å; V2–O11 (protonated, equatorial site), 2.026(5) Å].[34] On the other hand, the *trans* effect contributing about 0.2 Å to the elongation of the $V–O_{\alpha\text{-hydroxy}}$ distance is also supported by the change of V–N distances, where the nitrogen atom on the *trans* position [2.316(2) Å] is longer than those of on the equatorial sites $[2.129(2)_{av}$ Å].

Based on the $Mo^{IV/III}$ and V^{III} proposed for FeMo-co and FeV-co,[73–76] the V/Mo–O(H) distances of α-hydroxycarboxylato vanadium/molybdenum complexes with different coordination modes and different oxidation states are listed in Table 1 for comparisons with FeV/Mo-cos. The protonated V^{IV}–$O_{α\text{-hydroxy}}$ distances [$2.210(5)_{av}$ Å] are the closest distances to the corresponding V–$O_{α\text{-hydroxy/α-alkoxy}}$ distance in homocitrato FeV-co (2.170_{av} and 2.160_{av} Å).[1,7] While the other deprotonated V–$O_{α\text{-alkoxy}}$ distances are shorter than that of FeV-co to different degrees, including the V^{IV}–$O_{α\text{-alkoxy}}$ distance [$1.925(4)_{av}$ Å], the pentavalent V^{V}–$O_{α\text{-alkoxy}}$ distance [$1.856(4)_{av}$ Å] in V_2O_3 cores, as well as the V–$O_{α\text{-alkoxy}}$ distances (~ 2.0 Å) in dimeric V_2O_2 or V_2O_4 units. The V^{V}–$O_{α\text{-alkoxy}}$ distances are shorter than the V^{IV}–$O_{α\text{-alkoxy}}$ distances due to the higher oxidation state of the metal center. The V–$O_{α\text{-alkoxy}}$ distances in V_2O_4 or V_2O_2 units are slightly longer than the aforementioned V^{IV}–$O_{α\text{-alkoxy}}$ and V^{V}–$O_{α\text{-alkoxy}}$ distances due to the bridging coordination modes, where the α-alkoxy group serves as bridging ligand. On the other hand, the distances between vanadium and α-carboxy groups (around 2.0 Å) are shorter than that of homocitrate in FeV-co (2.112_{av} and 2.104_{av} Å).[1,7]

From the Table 1, the protonated Mo–$O_{α\text{-hydroxy}}$ distances of α-hydroxycarboxylato molybdenum complexes are about 0.2 Å longer than those of deprotonated Mo–$O_{α\text{-alkoxy}}$ bonds as described previously.[3] The Mo^{IV}–$O_{α\text{-hydroxy}}$ distances of 2.179(4) Å and 2.228(4) Å in $[Mo^{IV}{}_3S_4(PPh_3)_3(Hlact)_2lact]$[67] are close to the value of 2.17_{av} Å in FeMo-co,[2] while the Mo^{IV}–$O_{α\text{-alkoxy}}$ distances of $2.022(3)_{av}$ Å in $Na_2[Mo_3SO_3(lact)_3(im)_3]\cdot 10H_2O$[3] are obviously shorter. This is also true for the Mo^{0}–$O_{α\text{-hydroxy}}$ (non-nature) bonds, which are the longest protonated distances due to their lowest oxidation states. In comparison with the bond distances of these similar compounds, the vanadium/molybdenum atoms in cofactors might have weak interactions with homocitrates and protonated α-hydroxy coordinations (Figure 2).

^{13}C NMR Measurement.

Solution ^{13}C NMR spectrum shown in Fig. 3 provides valuable information on the coordination environment and chemical behavior of **1**. The resonances for α-carboxy (α-CO_2) and α-hydroxy (α-COH) groups in **1** are at around 178.9 and 61.9 ppm respectively, showing downfield shifts compared with free glycolic acid (α-CO_2 177.0 ppm; α-≡COH 60.2 ppm). The small shifts indicated that the protonated coordination environment of glycolate ligand in **1** was close to the free state, which implies a weak coordination between oxidovanadium ion and α-hydroxy group.

FT-IR Measurements.

The FT-infrared spectra of the solids **1** and **2** in the regions of 1800–400 cm^{-1} are shown in Fig. 4 and the spectrum for **3** is shown in Figure S7. To eliminate the interference peaks from bipyridine and phenanthroline, the IR spectra of previously reported complexes $[VO(phen)_2Cl]Cl\cdot H_2O$[77] and $[VO_2(bpy)_2]Cl\cdot 4H_2O$[78] were also re-recorded (Fig. 4). The spectra of **1** ~ **3** show well-resolved strong and sharp absorption bands for the carboxy groups of coordinated glycolates. For **1** and **2**, the asymmetric stretching vibrations $\nu_{as}(CO_2^-)$ are observed at 1600 and 1607 cm^{-1} and the corresponding symmetric stretching vibrations $\nu_s(CO_2^-)$ appear at 1390 and 1377 cm^{-1} respectively. For **3**, the asymmetric

stretching vibrations $\nu_{as}(CO_2^-)$ are observed at 1655, 1649, 1630, 1597, 1561 and 1554 cm $^{-1}$. The corresponding symmetric stretches $\nu_s(CO_2^-)$ appear at 1421, 1412, 1356 and 1317 cm^{-1}. All of the carboxy absorptions shift to lower frequencies in comparison with those of free ligand H_2glyc. The frequency differences $\Delta[\nu_{as}(CO_2^-)\text{-}\nu_s(CO_2^-)]$[79] are greater than 200 cm^{-1}, which are consistent with the monodentate fashion that the carboxy group is coordinated to the metal ion, and are in agreement with the structural data observed with X-ray crystallography. The vibrational bands above 2000 cm^{-1} are assigned to C−H, N−H and O−H stretching modes. The features in the region of 920–990 cm^{-1} indicate the existence of V=O bond, and are consistent with the values observed in other vanadium complexes.[38,41,43,80,81]

The C–O stretching vibrations in alcohols produce bands in the region 1260–1000 cm^{-1}.[82] Based on the observations on some alcohols and α-hydroxycarboxylic acids listed in Table S7, the peaks of **1** at 1051.3 and 1039.5 cm^{-1} are assigned to the protonated C–OH stretching vibrations, while the peaks of **2** at higher frequencies 1074.4 and 1061.0 cm^{-1} are assigned to the deprotonated C–O stretching vibrations.[65] All of the C–O(H) absorptions were shifted to lower frequencies in comparison with H_2glyc at 1086 cm^{-1}. The comparison of the IR spectra for **1**, **2**, $[VO(phen)_2Cl]Cl{\cdot}H_2O$[77] and $[VO_2(bpy)_2]Cl{\cdot}4H_2O$[78] also supports the assignments for the peaks in Fig. 4. The protonated glycolato oxidovanadium complex **1** shows a red-shift (about 23 cm^{-1}) in comparison with the deprotonated glycolato oxidovanadium complex **2**. Besides, theoretical frequency calculations using Gaussian 09 for **1** and **2** (Figure S8) also exhibit the same red-shift trend, which show ν(C–O) and ν(C–OH) at 1098 and 1036 cm^{-1} respectively. This is the first time a similar pair of protonated and deprotonated complexes with the same V-homocitrate local coordination structure was investigated.

In Fig. S7 the C–O stretching vibrations of **3** are more complex due to the multiple types of coordination of glycolates. Complex **3** containing both α-alkoxy and α-hydroxy groups exhibits two absorptions at 1088.3 and 1064.5 cm^{-1}, which are preliminarily assigned to the deprotonated $C\text{–}O_{\alpha\text{-alkoxy}}$ and protonated $C\text{–}O_{\alpha\text{-hydroxy}}$ stretching vibrations respectively. Therefore, complex **3** can serve as a mixed-(de)protonated model compound for the coexisting state of protonated and deprotonated homocitrates in nitrogenase.

Table 2 shows characteristic peaks of C–O or C–OH stretching vibrations of α-hydroxycarboxylato vanadium and molybdenum complexes, which serve as model compounds for FeV-co and FeMo-co. In analyzing these C–O/C–OH stretching vibrations, we have found that, whether in vanadium or molybdenum complexes, the protonated C–OH stretching vibrational frequencies are generally lower than the deprotonated C–O stretching vibrations. For example, previously reported lactato molybdenum(IV) complexes $Na_2[Mo_3SO_3(lact)_3(im)_3]{\cdot}10H_2O$[3] with α-alkoxy coordination and $[Mo^{IV}{}_3S_4(PPh_3)_3(Hlact)_2lact]$[67] with α-alkoxy/α-hydroxy coordinations also show red-shift from 1095.4, 1060.8, 1049.9 to 1090, 1036 cm^{-1} respectively. In brief, the ν(C–OH) of these complexes can be as low as 1030 cm^{-1}, or even shifted to 1005 cm^{-1}, while ν(C–O) are almost around 1080 cm^{-1}. This is because the protonation weakens the strength of the C–O bond, resulting in the red-shift of vibrational frequency. As we can see in Table 2, the $C\text{–}O_{\alpha\text{-hydroxy}}$ distances (1.44_{av} Å) of protonated compounds are subtly longer than C

$-O_{\alpha\text{-alkoxy}}$ distances of deprotonated compounds (1.415_{av} Å), and comparable with those of FeV-co (1.443_{av} Å) and FeMo-co (1.449_{av} Å). This is in accordance with the proposition of α-hydroxy coordination models in cofactors. The $C–O_{\alpha\text{-alkoxy}}$ vibrational frequencies of deprotonated homocitrate model complexes, $[V_2O_3(phen)_3(R,S\text{-}H_2homocit)_2(H_2O)]Cl\cdot 6H_2O$[41] and $K_2[Mo^{VI}O_2(R,S\text{-}H_2homocit)_2]\cdot 2H_2O$[61] were both observed to have an IR peak at 1084 cm^{-1}. Although model complexes of protonated Mo/V homocitrates have not yet been obtained, the corresponding IR absorptions of the $C-O_{\alpha\text{-hydroxy}}$ bonds should shift to lower wave numbers according to the Hook law.

Re-evaluation of IR Spectrum of extracted FeMo-co.

To identify the protonation state of homocitrate in FeMo-co, we have re-examined the IR spectrum of FeMo-co extracted from nitrogenase purified from *Azotobacter vinelandii* (Fig. 5). The IR spectrum for the film sample of extracted FeMo-co exhibits absorption peaks at 1672, 1606, 1483, 1457, 1399, 1375, 1332, 1319, 1242, 1183, 1084, 1031, 1006, 984, 801, 748, 698, 647, 614 and 578 cm^{-1} respectively. Qualitative assignments of extracted FeMo-co are given in Table 3, where the vibrations of the following groups: COO^-, C–C, C–O, Mo–O, tetraethylammonium chloride (TEAC) and N-methylformamide (NMF) are identified. The IR spectrum for TEAC is also shown in Fig. 5.

The complexes' C–O(H) stretching frequencies in Table 2 can serve as references for the C–O(H) vibrations in FeMo-co. The oxidation state of Mo atom in FeMo-co was assigned as Mo(IV)[74] and Mo(III)[75,76] previously, which are close to those of Mo(IV) complexes, such as $Na_2[Mo^{IV}{}_3SO_3(R,S\text{-lact})_3(im)_3]\cdot 10H_2O$[3] and $[Mo^{IV}{}_3S_4(PPh_3)_3(Hlact)_2lact]$.[67] Therefore the C–OH or C–O vibrational frequency of FeMo-co is inferred to be around 1030 cm^{-1} or 1080 cm^{-1} respectively, which are analogous to the assignments of C–OH or C–O vibrations in complexes **1** and **2**.

The peak at 1672 cm^{-1} in extracted FeMo-co IR is assigned to the asymmetric vibration $\nu_{as}(CO_2^-)$ of homocitrate, in comparison with 1675 cm^{-1} for $K_2[Mo^{VI}O_2(R,S\text{-}H_2homocit)_2]\cdot 2H_2O$.[61] It was assigned only to NMF in the previous reference.[9] We therefore assign this peak to $\nu_{as}(CO_2^-)$ of extracted FeMo-co and the NMF absorptions.

The peak at 1606 cm^{-1} is assigned to the asymmetric vibration $\nu_{as}(CO_2^-)$ for homocitrate in extracted FeMo-co, corresponding to 1589 cm^{-1} for $K_2[Mo^{VI}O_2(R,S\text{-}H_2homocit)_2]\cdot 2H_2O$[61] and 1607 cm^{-1} for $[V_2O_3(phen)_3\ (R,S\text{-}H_2homocit)_2(H_2O)]Cl\cdot 6H_2O$[41]. This is consistent with the previous assignment by Orme-Johnson and coworkers[9], but with a clearer resolution.

The peaks at 1399 and 1375 cm^{-1} for extracted FeMo-co should belong to the symmetric carboxyl vibrations, in comparison with the peaks 1390 cm^{-1} for $K_2[Mo^{VI}O_2(R,S\text{-}H_2homocit)_2]\cdot 2H_2O$[61] and 1383 and 1346 cm^{-1} for $[V_2O_3(phen)_3(R,S\text{-}H_2homocit)_2(H_2O)]Cl\cdot 6H_2O$,[41] which are consistent with Orme-Johnson's observation.[9] But the peaks in the range of 1493 ~ 1375 cm^{-1} also overlap with strong absorptions of TEAC, therefore 1399 and 1375 cm^{-1} could be assigned to $\nu_s(CO_2^-)$ of extracted FeMo-co and the TEAC absorptions.

The peak at 1183 cm^{-1} for extracted FeMo-co is assigned to C–C vibration, while the 578 cm^{-1} peak in the FeMo-co spectrum is assigned to Mo–O vibration in comparison with 553 and 540 cm^{-1} in $K_2[Mo^{VI}O_2(R,S\text{-}H_2homocit)_2]\cdot 2H_2O$.[61] The strong peaks at 1006 and 801 cm^{-1} are assigned to the vibrations of TEAC.

Most importantly, the peaks at 1083 and 1031 cm^{-1} in the IR-spectrum of extracted FeMo-co are assigned to C–O and C–OH vibrations as mentioned in the beginning of this section. The absorption at 1031 cm^{-1} is corresponding to the protonated C–OH at 1051, 1039 cm^{-1} in **1**, 1032 cm^{-1} in $[V^{IV}O(H_2cit)(bpy)]\cdot 2H_2O$,[34] 1036 cm^{-1} in $[Mo^{IV}{}_3S_4(PPh_3)_3(Hlact)_2(lact)]$[62] respectively. The peak at 1083 cm^{-1} is corresponding to the deprotonated model compounds $[V^{IV/V}{}_2O_3(phen)_3(R,S\text{-}H_2homocit)_2(H_2O)]Cl\cdot 6H_2O$[41] (1084 cm^{-1}) and $K_2[Mo^{VI}O_2(R,S\text{-}H_2homocit)_2]\cdot 2H_2O$[61] (1084 cm^{-1}). Therefore, protonated and deprotonated homocitrates coexist in the particular extracted FeMo-co film evaluated here.

CONCLUSIONS

Here report a pair of mononuclear protonated and deprotonated glycolato oxidovanadium complexes with similar bidentate chelated local structure of V-homocitrate: $[VO(Hglyc)(phen)(H_2O)]Cl\cdot 2H_2O$ (**1**) and $[VO(glyc)(bpy)(H_2O)]$ (**2**). The glycolate ligand coordinated bidentately to the central vanadium with protonated α-hydroxy and α-carboxy oxygen atoms in **1**, while coordinated with deprotonated α-alkoxy and α-carboxy oxygen atoms in **2**. In oxidovanadium triglycolate $(NH_4)_2[VO(Hglyc)_2(glyc)]\cdot H_2O$ (**3**), the glycolate ligands coordinated to vanadium through protonated α-hydroxy, deprotonated α-alkoxy and α-carboxy groups. The crystal structural data show that the elongated protonated V/Mo $-O_{\alpha\text{-hydroxy}}$ distances are close to those of FeV/Mo-cos, which indicate a proposed protonated α-hydroxy group in FeV/Mo-cos.

Based on the comparisons of $C-O_{\alpha\text{-alkoxy}/\alpha\text{-hydroxy}}$ stretching vibrations of vanadium and molybdenum complexes, the C–OH stretching vibration will shift to a lower wave number in comparison with C–O stretching vibrations. The IR spectrum for extracted FeMo-co shows two absorption peaks at 1084 and 1031 cm^{-1}, indicating a co-existence of deprotonated α-alkoxy and protonated α-hydroxy coordination in the Mo-homocitrate of FeMo-co. The IR spectra for some of the previously reported Mo/V complexes were also cited to compare with the three special oxidovanadium complexes in this publication and with the extracted FeMo-co. Nevertheless, the ≡C–O(H) peaks are assigned for the first time for all these samples.

EXPERIMENTAL SECTION

Materials and Instrumentation.

All solvents and reagents (in commercially analytical grade) were used without further purification. The pH value was determined by a PHB-8 digital pH meter. Elemental analyses (for C, H and N) were performed with a Vario EL III CHN elemental analyzer. Infrared spectra were measured in the range 400−4000 cm^{-1} on a Nicolet FT-IR spectrometer with samples in KBr plates. The solid diffused UV/Vis spectra were recorded at 293K using a

Cary 5000 UV-visible-NIR spectrophotometer in the 200−800 nm range. Solid and solution (in DMSO) electron paramagnetic resonance (EPR) spectra were obtained by a Bruker EMX-10/12 spectrometer using crystalline samples at low temperatures. The FTIR of extracted FeMo-co was measured using Bruker V66/S and V70/v FTIR spectrometers at UCD and LBNL, with FeMo-co film on ZnSe or polyethylene plates respectively for different wave number regions. To minimize the NMF amount left in the FeMo-co film, the samples were pumped for more than 8 hrs before the measurement. Solution ^{13}C NMR spectrum of **1** with long time superimposition was recorded on a Bruker Avance III 600MHz NMR spectrometer with D_2O, using DSS (sodium 2,2-dimethyl-2-silapentane-5-sulfonate) as an internal reference.

Cell Growth and Purification of Nitrogenase Proteins.

The *Av* wild-type strain was grown in the absence of a fixed-nitrogen source in a 24-L fermenter at 30 °C in a modified, liquid Burk medium.[83] All cultures contained 20 μM $FeCl_3$ and 10 μM Na_2MoO_4 and were grown to a final cell density of 250 Klett units recorded on a Klett–Summerson meter equipped with a number 54 filter. All manipulations of nitrogenase proteins were performed anaerobically using either a Schlenk line or an anaerobic glovebox operating at less than 1 ppm O_2. After harvesting, cell extracts were prepared by diluting the whole cells with an equal amount of 50 mM Tris pH 8.0 buffer prior to passing through a French pressure cell and a centrifuge at 98000 g for 90 min. Nitrogenase component proteins were separated by anaerobic Q-Sepharose anion exchange column chromatography using a linear NaCl concentration gradient. *Av*2 was purified to homogeneity by fractionation from a second Q-Sepharose column. *Av*1 was further purified by Sephacryl S-200 gel filtration and phenyl-Sepharose hydrophobic-interaction chromatography.[84] The purified Nitrogenase proteins were concentrated individually using an Amicon microfiltration pressure concentrator before buffer exchange to 25 mM HEPES pH 7.5, 100 mM NaCl, 10 mM $MgCl_2$, and 2 mM $Na_2S_2O_4$ by dialysis at 4 °C. Purified wild-type *Av*1 had specific activities of 2200 nmol of H_2 (min·mg·protein)$^{-1}$ at 30 °C, when assayed in the presence of an optimal amount of the purified complementary component protein as described previously.[84] Protein concentrations were determined by the Lowry method.

Extraction of FeMo-co from *Av*1.

*Av*1 was purified as above through the gel-filtration step, yielding protein with a specific activity of ~1000 nmol of H_2 (min·mg protein)$^{-1}$ and a Mo content of ~1 g·atom per mol of *Av*1. After dialysis to lower the NaCl concentration, the *Av*1 was loaded onto a DE-52 cellulose column that had been washed with 50 mM Tris pH 7.4 buffer containing 2 mM $Na_2S_2O_4$. The bound protein was washed with N,N-dimethylformamide containing 50 mM 2,2′- bipyridine, 5 mM phosphate buffer pH 8, with 2 mM $Na_2S_2O_4$, and water (ca. 5% v/v) until the noncofactor iron was completely eluted. The column was then washed with N-methylformamide (NMF) containing 5 mM phosphate buffer pH 8, with 2 mM $Na_2S_2O_4$, and water (ca. 5% v/v), and FeMoco was then eluted with NMF that contained 500 mM tetraethylammonium chloride, 5 mM phosphate buffer pH 8, with 2 mM $Na_2S_2O_4$, and water (ca. 5% v/v). The eluted FeMo-co was concentrated approximately 20-fold by distilling off the NMF under vacuum at 40 °C. FeMo-co was assayed[85] by reconstitution of the DJ42 *Av*

strain, which has a deletion for the FeMo-co biosynthetic genes *nif*ENX. The FeMo-co used in this study activated a DJ42 crude extract and produced 75 nmol of H_2 (min·mg protein)$^{-1}$.

X-Ray Crystallography.

The crystal structural data for **1** ~ **3** were collected on an Oxford Gemini CCD diffractometer, with graphite monochromatic Mo-Kα radiation (λ = 0.71073 Å) at 173 K. Muti-scan absorption corrections were applied. Direct methods structure solution, difference Fourier calculations, and full-matrix least-squares refinements against F^2 were performed with SHELXL-2018/3 using the OLEX2 crystallographic software package[86–88]. All non-hydrogen atoms were refined anisotropically, while the hydrogen atoms of carbon atoms were generated geometrically and the hydrogen atoms of water molecules, ammonium ions and hydroxyl groups were located from differential Fourier maps and refined isotropically. To obtain reasonable structures, some "dfix" restraints were applied to the water molecules and hydroxyl group. The distances of O–H were restrained to be 0.85 Å: O1w–H1wA, O1w–H1wB, O2w–H1wA, O2w–H1wB, O3w–H1wA, O3w–H1wB and O1–H1 in **1**, O1w–H1wA, O1w–H1wB in **2**. The angles of H–O–H were restrained by fixing the distances of the two hydrogen atoms at 1.39 Å: H1wA…H1wB, H2wA…H2Wb and H3wA…H3wB in **1**.

Computational method.

The geometry optimizations and frequency calculations were carried out using Gaussian 09.[89] The molecular structures of $[VO(Hglyc)(phen)(H_2O)]^+$ cation of **1** and neutral molecule of **2** were optimized separately using DFT method. The 6–31G* (d, p) basis set was used for all atoms and B3LYP exchange–correlation functional was utilized to evaluate their performances in reproducing the solid-state structures and spectroscopic properties.

Synthesis of $[VO(Hglyc)(phen)(H_2O)]Cl{\cdot}2H_2O$ (1).

Vanadium pentoxide V_2O_5 (0.091 g, 0.50 mmol), glycolic acid in excess (0.60 g, 8.0 mmol), and 1,10-phenanthroline (0.10 g, 0.51 mmol) were dissolved in water (8 mL) with continuous stirring. The pH value was adjusted to 1.0 with dilute hydrochloric acid (1.0 M). The mixture was placed in a Teflon-lined stainless steel bomb. The bomb was heated to 443 K for 3 days and cooled with programmed control. The bluish green solution was evperated at room temperature for two months to grow blue crystals. The crystals were collected and washed with ethanol to afford **1** (0.067 g, 32% yield based on phen). Elemental analysis (calc. for $C_{14}H_{11}ClN_2O_7V$): C, 40.8; H, 4.2; N, 6.8%. Found: C, 40.6; H, 4.0; N, 6.4%. IR (cm^{-1}): 3435(s), 3367(s), 3230(s), 3096(s), 3061(s), 2665(s), 2595(s), 2135(m), 2002(w), 1966(w), 1934(w), 1600(vs), 1522(s), 1493(m), 1426(s), 1390(s), 1341(m), 1303(m), 1220(w), 1211(w), 1200(w), 1151(w), 1141(w), 1109(m), 1051(m), 1041(w), 985(s), 940(m), 912(w), 875(m), 850(m), 799(w), 777(m), 742(m), 723(s), 654(m), 579(m), 559(m), 515(m), 500(m), 487(m), 435(m).

Synthesis of $[VO(glyc)(bpy)(H_2O)]$ (2).

Vanadium pentoxide V_2O_5 (0.091 g, 0.50 mmol), glycolic acid in excess (0.40 g, 5.26 mmol), and 2,2'-bipyridine (0.080 g, 0.50 mmol) were dissolved in water (8.0 mL) with

continuous stirring. The pH value was adjusted to 3.0 with dilute potassium hydroxide (1.0 M). The bomb was heated to 443 K for 3 days and cooled with programmed control. The brown green crystals were collected and washed with ethanol to afford **2** (0.090 g, 56% yield based on bpy). Elemental analysis (calc for $C_{12}H_{12}N_2O_5V$): C, 45.7; H, 3.8; N, 8.9%. Found: C, 45.4; H, 3.6; N, 8.5%. IR (cm^{-1}): 3435(m), 3111(m), 3100(m), 3057(m), 3033(m), 2863(m), 2829(m), 1607(vs), 1575(m), 1492(m), 1474(m), 1442(s), 1377(s), 1324(m), 1314(m), 1246(w), 1226(w), 1174(w), 1157(w), 1100(w), 1074(s), 1061(m), 1044(w), 1024(m), 1012(w), 968(s), 919(m), 769(s), 736(s), 653(m), 632(m), 596(m), 575(m), 520(m), 483(w), 443(w), 425(w).

Synthesis of $(NH_4)_2[VO(Hglyc)_2(glyc)]\cdot H_2O$ (3).[24,25]

Oxidovanadium sulfate (326 mg, 2.0 mmol) and glycolic acid (456 mg, 6.0 mmol) were dissolved in water (5.0 mL). The pH value of the solution was adjusted to 5.0 by concentrated ammonium hydroxide with continuous stirring. After one month, the light purple precipitate was collected and washed with water and ethanol to afford **3**. (0.174g, 25% yield based on vanadium). Anal. Calc. for $C_6H_{18}N_2O_{11}V$: C, 20.9; H, 5.3; N, 8.1. Found: C, 20.8; H, 5.5; N, 8.0 (%). IR (cm^{-1}): 3399(m), 3180(s), 3053(s), 2914(m), 2840(m), 1655(s), 1649(s), 1630(s), 1597(m), 1561(s), 1554(s), 1502(w), 1465(m), 1449(m), 1421(s), 1412(s), 1356(s), 1317(s), 1247(w), 1237(w), 1088(s), 1065(s), 1006(w), 955(s), 935(s), 740(m), 716(m), 603(m), 583(m), 568(m), 522(s), 483(w), 477(w), 444(m), 432(m), 419(m).

Supplementary Material

Refer to Web version on PubMed Central for supplementary material.

ACKNOWLEDGMENT

We thank the supports from the National Science Foundation (21773196), the National Science Foundation of Fujian (2016I0101) and NIH GM-65440 (S.P.C.) for their generous financial supports. What's more, we thank Ms. La-Jia Yu in EPR measurements.

ABBREVIATIONS

FeMo-co	FeMo-cofactor
H_4homocit	homocitric acid
FeV-co	VFe-cofactor
phen	phenanthroline
H_2glyc	glycollic acid
bpy	bipyridine
TEAC	tetraethylammonium chloride

REFERENCES

(1). Sippel D; Einsle O The structure of vanadium nitrogenase reveals an unusual bridging ligand, Nat. Chem. Biol 2017, 13, 956–960. [PubMed: 28692069]

(2). Spatzal T; Aksoyoglu M; Zhang L; Andrade SLA; Schleicher E; Weber S; Rees DC; Einsle O Evidence for interstitial carbon in nitrogenase FeMo cofactor, Science 2011, 334, 940. [PubMed: 22096190]

(3). Wang SY; Jin WT; Chen HB; Zhou ZH Comparison of hydroxycarboxylato imidazole molybdenum(iv) complexes and nitrogenase protein structures: indirect evidence for the protonation of homocitrato FeMo-cofactors, Dalton Trans 2018, 47, 7412–7421. [PubMed: 29786717]

(4). Lancaster KM; Roemelt M; Ettenhuber P; Hu Y; Ribbe MW; Neese F; Bergmann U; DeBeer S X-ray emission spectroscopy evidences a central carbon in the nitrogenase iron-molybdenum cofactor, Science 2011, 334, 974–977. [PubMed: 22096198]

(5). Einsle O; Tezcan FA; Andrade SL; Schmid B; Yoshida M; Howard JB; Rees DC Nitrogenase MoFe-protein at 1.16 Å resolution: a central ligand in the FeMo-cofactor, Science 2002, 297, 1696–1700. [PubMed: 12215645]

(6). Kim J; Rees DC Structural models for the metal centers in the nitrogenase molybdenum-iron protein, Science 1992, 257, 1677–1682. [PubMed: 1529354]

(7). Sippel D; Rohde M; Netzer J; Trncik C; Gies J; Grunau K; Djurdjevic I; Decamps L; Andrade SLA A bound reaction intermediate sheds light on the mechanism of nitrogenase, Science 2018, 359, 1484–1489. [PubMed: 29599235]

(8). Schmid B; Ribbe MW; Einsle O; Yoshida M; Thomas LM; Dean DR; Rees DC; Burgess BK Structure of a cofactor-deficient nitrogenase MoFe protein, Science 2002, 296, 352–356. [PubMed: 11951047]

(9). Walters MA; Chapman SK; Orme-Johnson WH The nature of amide ligation to the metal sites of FeMoco (iron-molybdenum cofactor), Polyhedron 1986, 5, 561–565.

(10). Levchenko L; Roschupkina O; Sadkov A; Marakushev S; Mikhailov G; Borod'ko YG Spectroscopic investigation of FeMo-cofactor. Coenzyme A as one of the probable components of an active site of nitrogenase, Biochem. Biophys. Res. Commun 1980, 96, 1384–1392. [PubMed: 6933992]

(11). Robinson AE; Richards AJ; Thomson AJ; Hawkes TR; Smith BE Low-temperature magnetic-circular-dichroism spectroscopy of the iron-molybdenum cofactor and the complementary cofactor-less MoFe protein of Klebsiella pneumoniae nitrogenase, Biochem. J 1984, 219, 495–503. [PubMed: 6378176]

(12). Stephens PJ; McKenna CE; McKenna MC; Nguyen HT; Devlin F Circular dichroism and magnetic circular dichroism of reduced molybdenum-iron protein of Azotobacter vinelandii nitrogenase, Biochemistry 1981, 20, 2857–2864. [PubMed: 6941811]

(13). Mascharak PK; Smith MC; Armstrong WH; Burgess BK; Holm RH Fluorine-19 chemical shifts as structural probes of metal-sulfur clusters and the cofactor of nitrogenase, Proc. Natl. Acad. Sci. USA 1982, 79, 7056–7060. [PubMed: 6960364]

(14). Conradson SD; Burgess BK; Newton WE; Di CA; Filipponi A; Wu ZY; Natoli CR; Hedman B; Hodgson KO Selenol binds to iron in nitrogenase iron-molybdenum cofactor: an extended x-ray absorption fine structure study, Proc. Natl. Acad. Sci. USA 1994, 91, 1290–1293. [PubMed: 8108404]

(15). Liu HI; Burgess BK; Natoli CR; Filipponi A; Gavini N; Hedman B; Di Cicco A; Hodgson KO EXAFS studies of FeMo-cofactor and MoFe protein: Direct evidence for the long-range Mo-Fe-Fe interaction and cyanide binding to the Mo in FeMo-cofactor, J. Am. Chem. Soc 1994, 116, 2418–2423.

(16). Conradson SD; Burgess BK; Newton WE; Mortenson LE; Hodgson KO Structural studies of the molybdenum site in the MoFe protein and its FeMo cofactor by EXAFS, J. Am. Chem. Soc 1987, 109, 7507–7515.

(17). Cramer SP; Gillum WO; Hodgson KO; Mortenson LE; Stiefel EI; Chisnell JR; Brill WJ; Shah VK The molybdenum site of nitrogenase. 2. A comparative study of molybdenum-iron proteins

and the iron-molybdenum cofactor by x-ray absorption spectroscopy, J. Am. Chem. Soc 1978, 100, 3814–3819.

(18). Antonio MR; Teo BK; Orme-Johnson WH; Nelson MJ; Groh SE; Lindahl PA; Kauzlarich SM; Averill BA Iron EXAFS of the iron-molybdenum cofactor of nitrogenase, J. Am. Chem. Soc 1982, 104, 4703–4705.

(19). Arber JM; Flood AC; Garner CD; Gormal CA; Hasnain SS; Smith BE Iron K-edge X-ray absorption spectroscopy of the iron-molybdenum cofactor of nitrogenase from Klebsiella pneumoniae, Biochem. J 1988, 252, 421–425. [PubMed: 3046607]

(20). Rawlings J; Shah VK; Chisnell JR; Brill WJ; Zimmermann R; Münck E; Orme-Johnson WH Novel metal cluster in the iron-molybdenum cofactor of nitrogenase. Spectroscopic evidence, J. Biol. Chem 1978, 253, 1001–1004. [PubMed: 203578]

(21). Newton WE; Gheller SF; Sands RH; Dunham WR Mössbauer spectroscopy applied to the oxidized and semi-reduced states of the iron-molybdenum cofactor of nitrogenase, Biochem. Biophys. Res. Commun 1989, 162, 882–891. [PubMed: 2757645]

(22). Lukoyanov D; Pelmenschikov V; Maeser N; Laryukhin M; Yang TC; Noodleman L; Dean DR; Case DA; Seefeldt LC; Hoffman BM Testing if the interstitial atom, X, of the nitrogenase molybdenum-iron cofactor is N or C: ENDOR, ESEEM, and DFT studies of the S = 3/2 resting state in multiple environments, Inorg. Chem 2007, 46, 11437–11449. [PubMed: 18027933]

(23). Yang TC; Maeser NK; Laryukhin M; Lee HI; Dean DR; Seefeldt LC; Hoffman BM The interstitial atom of the nitrogenase FeMo-cofactor: ENDOR and ESEEM evidence that it is not a nitrogen, J. Am. Chem. Soc 2005, 127, 12804–12805. [PubMed: 16159266]

(24). Delfino I; Cerullo G; Cannistraro S; Manzoni C; Polli D; Dapper C; Newton WE; Guo Y; Cramer SP Observation of terahertz vibrations in the nitrogenase FeMo cofactor by femtosecond pump-probe spectroscopy, Angew. Chem. Int. Ed. Engl 2010, 122, 4004–4007.

(25). Xiao Y; Fisher K; Smith MC; Newton WE; Case DA; George SJ; Wang H; Sturhahn W; Alp EE; Zhao J; Yoda Y; Cramer SP How Nitrogenase Shakes − Initial Information about P−Cluster and FeMo-cofactor Normal Modes from Nuclear Resonance Vibrational Spectroscopy (NRVS), J. Am. Chem. Soc 2006, 128, 7608–7612. [PubMed: 16756317]

(26). George SJ; Igarashi RY; Xiao Y; Hernandez JA; Demuez M; Zhao D; Yoda Y; Ludden PW; Rubio LM; Cramer SP Extended X-ray absorption fine structure and nuclear resonance vibrational spectroscopy reveal that *NifB*-co, a FeMo-co precursor, comprises a 6Fe core with an interstitial light atom, J. Am. Chem. Soc 2008, 130, 5673–5680. [PubMed: 18386899]

(27). Shah VK; Brill WJ Isolation of a molybdenum--iron cluster from nitrogenase, Proc. Natl. Acad. Sci. USA 1981, 78, 3438–3440. [PubMed: 6267591]

(28). Lee H-I; Hales BJ; Hoffman BM Metal-Ion Valencies of the FeMo Cofactor in CO-Inhibited and Resting State Nitrogenase by 57Fe Q-Band ENDOR, J. Am. Chem. Soc 1997, 119, 11395–11400.

(29). Yoo SJ; Angove HC; Papaefthymiou V; Burgess BK; Münck E Mössbauer Study of the MoFe Protein of Nitrogenase from Azotobacter vinelandii Using Selective 57Fe Enrichment of the M-Centers, J. Am. Chem. Soc 2000, 122, 4926–4936.

(30). Harris TV; Szilagyi RK Comparative Assessment of the Composition and Charge State of Nitrogenase FeMo-Cofactor, Inorg. Chem 2011, 50, 4811–4824. [PubMed: 21545160]

(31). Bjornsson R; Neese F; DeBeer S Revisiting the Mössbauer Isomer Shifts of the FeMoco Cluster of Nitrogenase and the Cofactor Charge, Inorg. Chem 2017, 56, 1470–1477. [PubMed: 28071903]

(32). Spatzal T; Schlesier J; Burger E-M; Sippel D; Zhang L; Andrade SLA; Rees DC; Einsle O Nitrogenase FeMoco investigated by spatially resolved anomalous dispersion refinement, Nature Communications 2016, 7, 10902.

(33). Cao ZX; Jin X; Zhou ZH; Zhang QE Protonation of metal-bound α-hydroxycarboxylate ligand and implication for the role of homocitrate in nitrogenase: computational study of the oxy-bidentate chelate ring opening, Int. J. Quantum Chem 2006, 106, 2161–2168.

(34). Chen CY; Chen ML; Chen HB; Wang HX; Cramer SP; Zhou ZH α-Hydroxy coordination of mononuclear vanadyl citrate, malate and S-citramalate with N-heterocycle ligand, implying a

new protonation pathway of iron-vanadium cofactor in nitrogenase, J. Inorg. Biochem 2014, 141, 114–120. [PubMed: 25240212]

(35). Benediktsson B; Bjornsson R QM/MM study of the nitrogenase MoFe protein resting state: broken-symmetry states, protonation states, and QM region convergence in the FeMoco active site, Inorg. Chem 2017, 56, 13417–13429. [PubMed: 29053260]

(36). Cao L; Caldararu O; Ryde U Protonation states of homocitrate and nearby residues in nitrogenase studied by computational methods and quantum refinement, J. Phy.Chem. B 2017, 121, 8242–8262.

(37). Siegbahn PEM A major structural change of the homocitrate ligand of probable importance for the nitrogenase mechanism, Inorg. Chem 2018, 57, 1090–1095. [PubMed: 29303565]

(38). Tsaramyrsi M; Kaliva M; Salifoglou A; Raptopoulou CP; Terzis A; Tangoulis V; Giapintzakis J Vanadium(IV)-citrate complex interconversions in aqueous solutions. A pH-dependent synthetic, structural, spectroscopic, and magnetic study, Inorg. Chem 2001, 40, 5772–5779. [PubMed: 11681884]

(39). Li X; Dai JW; Wang HX; Wu AA; Zhou ZH Chiral and achiral vanadyl lactates with vibrational circular dichroism: Toward the chiral metal cluster in nitrogenase, Inorg. Chim. Acta 2016, 453, 501–506.

(40). Jin WT; Li X; Zhou ZH Degradations of novel tetranuclear vanadyl glycollates to dinuclear species, Polyhedron 2017, 122, 99–104.

(41). Chen CY; Zhou ZH; Chen HB; Huang PQ; Tsai KR; Chow YL Formations of mixed-valence oxovanadiumV,IV citrates and homocitrate with N-heterocycle chelated ligand, Inorg. Chem 2008, 47, 8714–8720. [PubMed: 18722422]

(42). Biagioli M; Strinna-Erre L; Micera G; Panzanelli A; Zema M Molecular structure, characterization and reactivity of dioxo complexes formed by vanadium(V) with α-hydroxycarboxylate ligands, Inorg. Chim. Acta 2000, 310, 1–9.

(43). Burojevic S; Shweky I; Bino A; Summers DA; Thompson RC Synthesis, structure and magnetic properties of an asymmetric dinuclear oxocitratovanadate(IV) complex, Inorg. Chim. Acta 1996, 251, 75–79.

(44). Zhou ZH; Wan HL; Hu SZ; Tsai KR Syntheses and structures of the potassium-ammonium dioxocitratovanadate(V) and sodium oxocitratovanadate(IV) dimers, Inorg. Chim. Acta 1995, 237, 193–197.

(45). Zhou ZH; Wang JZ; Wan HL; Tsai KR Synthesis and structure of (NH4)2[V2O4(OCH2COO)2], Chem. Res. Chin. Univ 1994, 10, 102–106.

(46). Wright DW; Humiston PA; Orme-Johnson WH; Davis WM A unique coordination mode for citrate and a transition metal: K2[V(O)2(C6H6O7)]2·4H2O, Inorg. Chem 1995, 34, 4194–4197.

(47). Zhou ZH; Yan WB; Wan HL; Tsai KR; Wang JZ; Hu SZ Metal-hydroxycarboxylate interactions: syntheses and structures of K2[VO2(C6H6O7)]2·4H2O and (NH4)2[VO2(C6H6O7)]2·2H2O, J. Chem. Crystallogr 1995, 25, 807–811.

(48). Tsaramyrsi M; Kavousanaki D; Raptopoulou CP; Terzis A; Salifoglou A Systematic synthesis, structural characterization, and reactivity studies of vanadium(V)-citrate anions [VO2(C6H6O7)]22-, isolated from aqueous solutions in the presence of different cations, Inorg. Chim. Acta 2001, 320, 47–59.

(49). Zhou ZH; Zhang H; Jiang YQ; Lin DH; Wan HL; Tsai KR Complexation between vanadium(V) and citrate: spectroscopic and structural characterization of a dinuclear vanadium(V) complex, Transition Met. Chem 1999, 24, 605–609.

(50). Kaliva M; Giannadaki T; Salifoglou A; Raptopoulou CP; Terzis A A new dinuclear vanadium(V)-citrate complex from aqueous solutions. synthetic, structural, spectroscopic, and pH-dependent studies in relevance to aqueous vanadium(V)-citrate speciation, Inorg. Chem 2002, 41, 3850–3858. [PubMed: 12132908]

(51). Kaliva M; Raptopoulou CP; Terzis A; Salifoglou A Systematic studies on pH-dependent transformations of dinuclear vanadium(V)-citrate complexes in aqueous solutions. A perspective relevance to aqueous vanadium(V)-citrate speciation, J. Inorg. Biochem 2003, 93, 161–173. [PubMed: 12576278]

(52). Wright DW; Chang RT; Mandal SK; Armstrong WH; Orme-Johnson WH A novel vanadium(V) homocitrate complex: synthesis, structure, and biological relevance of [K2(H2O)5][(VO2)2(R,S-homocitrate)2]·H2O, J. Biol. Inorg. Chem 1996, 1, 143–151.

(53). Zhou ZH; Hou SY; Cao ZX; Wan HL; Ng SW Syntheses, crystal structures and biological relevance of glycolato and S-lactato molybdates, J. Inorg. Biochem 2004, 98, 1037–1044. [PubMed: 15149813]

(54). Zhou ZH; Yan WB; Wan HL; Tsai KR Synthesis and characterization of homochiral polymeric S-malato molybdate(VI): toward the potentially stereospecific formation and absolute configuration of iron-molybdenum cofactor in nitrogenase, J. Inorg. Biochem 2002, 90, 137–143. [PubMed: 12031805]

(55). Knobler CB; Wilson AJ; Hider RN; Jensen IW; Penfold BR; Robinson WT; Wilkins CJ Molybdenum(VI) complexes with malic acid: their inter-relationships, and the crystal structure of dicaesium bis[(S)-malato(2-)]-cis-dioxomolybdate(VI)-water (1/1), Dalton Trans 1983, 7, 1299–1303.

(56). Zhou ZH; Wan HL; Tsai KR Syntheses and spectroscopic and structural characterization of molybdenum(VI) citrato monomeric raceme and dimer, K4[MoO3(cit)]·2H2O and K4[(MoO2)2O(Hcit)2]·4H2O, Inorg. Chem 2000, 39, 59–64. [PubMed: 11229034]

(57). Zhang RH; Zhou XW; Guo YC; Chen ML; Cao ZX; Chow YL; Zhou ZH Crystalline and solution chemistry of tetrameric and dimeric molybdenum(VI) citrato complexes, Inorg. Chim. Acta 2013, 406, 27–36.

(58). Zhou ZH; Chen CY; Cao ZX; Tsai KR; Chow YL N-heterocycle chelated oxomolybdenum(VI and V) complexes with bidentate citrate, Dalton Trans 2008, 252, 2475–2479.

(59). Zhou ZH; Deng YF; Cao ZX; Zhang RH; Chow YL Dimeric dioxomolybdenum(VI) and oxomolybdenum(V) complexes with citrate at very low pH and neutral conditions, Inorg. Chem 2005, 44, 6912–6914. [PubMed: 16180846]

(60). Zhou ZH; Hou SY; Cao ZX; Tsai KR; Chow YL Syntheses, spectroscopies and structures of molybdenum(VI) complexes with homocitrate, Inorg. Chem 2006, 45, 8447–8451. [PubMed: 16999446]

(61). Zhou ZH; Wang H. x.; Yu P; Olmstead MM; Cramer SP Structure and spectroscopy of a bidentate bis-homocitrate dioxo-molybdenum(VI) complex: Insights relevant to the structure and properties of the FeMo-cofactor in nitrogenase, J. Inorg. Biochem 2013, 118, 100–106. [PubMed: 23147649]

(62). Li DM; Xing YH; Li ZC; Xu JQ; Song WB; Wang TG; Yang GD; Hu NH; Jia HQ; Zhang HM Synthesis and characterization of binuclear molybdenum–polycarboxylate complexes with sulfur bridges, J. Inorg. Biochem 2005, 99, 1602–1610. [PubMed: 15951017]

(63). Xing YH; Xu JQ; Sun HR; Li DM; Xing Y; Lin YH; Jia HQ A new dinuclear molybdenum(V)-sulfur complex containing citrate ligand: Synthesis and characterization of K2.5Na2NH4[Mo2O2S2(cit)2]·5H2O, Eur. J. Solid State Inorg. Chem 1998, 35, 745–756.

(64). Huang JL; Zhou KJ; Lu J The crystal and molecular structure of dipotassium tris(hydroxyacetato)vanadyl(IV) monohydrate, Sci. Sin., Ser. B 1986, 29, 1–7.

(65). Guilherme LR; Massabni AC; Cuin A; Oliveira LAA; Castellano EE; Heinrich TA; Costa-Neto CM Synthesis, characterization, crystal structure, and biological studies of vanadium complexes with glycolic acid, J. Coord. Chem 2009, 62, 1561–1571.

(66). Jodaian V; Mirzaei M; Arca M; Carla Aragoni M; Lippolis V; Tavakoli E; Langeroodi NS First example of a 1:1 vanadium(IV)-citrate complex featuring the 2,2'-bipyridine co-ligand: Synthesis, X-ray crystal structure and DFT calculations, Inorg. Chim. Acta 2013, 400, 107–114.

(67). Sokolov MN; Adonin SA; Virovets AV; Abramov PA; Vicent C; Llusar R; Fedin VP Complexes of M3S44+ (M = Mo, W) with chiral alpha-hydroxy and aminoacids: Synthesis, structure and solution studies, Inorg. Chim. Acta 2013, 395, 11–18.

(68). Takuma M; Ohki Y; Tatsumi K Molybdenum carbonyl complexes with citrate and its relevant carboxylates, Organometallics 2005, 24, 1344–1347.

(69). Fay AW; Lee CC; Wiig JA; Hu Y; Ribbe MW In Nitrogen Fixation: Methods and Protocols; Ribbe MW, Ed.; Humana Press: Totowa, NJ, 2011; pp 239–248.

(70). Shah VK; Brill WJ Isolation of an iron-molybdenum cofactor from nitrogenase, Proc. Natl. Acad. Sci. USA 1977, 74, 3249–3253. [PubMed: 410019]

(71). Brese NE; O'keeffe M Bond-valence parameters for solids, Acta Cryst 1991, B47, 192–197.

(72). Brown ID The chemical bond in inorganic chemistry: the bond valence model Oxford University Press on Demand: 2002; Vol. 12.

(73). Rees JA; Bjornsson R; Kowalska JK; Lima FA; Schlesier J; Sippel D; Weyhermueller T; Einsle O; Kovacs JA; De Beer S Comparative electronic structures of nitrogenase FeMoco and FeVco, Dalton Trans 2017, 46, 2445–2455. [PubMed: 28154874]

(74). True AE; McLean P; Nelson MJ; Orme-Johnson W; Hoffman BM Comparison of wild-type and nifV mutant molybdenum-iron proteins of nitrogenase from Klebsiella pneumoniae by ENDOR spectroscopy, J. Am. Chem. Soc 1990, 112, 651–657.

(75). Bjornsson R; Lima FA; Spatzal T; Weyhermuller T; Glatzel P; Bill E; Einsle O; Neese F; DeBeer S Identification of a spin-coupled Mo(III) in the nitrogenase iron-molybdenum cofactor, Chem. Sci 2014, 5, 3096–3103.

(76). Bjornsson R; Neese F; Schrock RR; Einsle O; DeBeer S The discovery of Mo(III) in FeMoco: reuniting enzyme and model chemistry, J. Biol. Inorg. Chem 2014, 20, 447–460. [PubMed: 25549604]

(77). Otieno T; Bond MR; Mokry LM; Walter RB; Carrano CJ Plasmid DNA cleavage by oxo-bridged vanadium(III) dimers without added co-oxidants or reductants, Chem. Comm 1996, 1, 37–38.

(78). Brand SG; Edelstein N; Hawkins CJ; Shalimoff G; Snow MR; Tiekink ERT An oxo-bridged binuclear vanadium(III) 2,2'-bipyridine complex and its vanadium(IV) and vanadium(V) oxidation products, Inorg. Chem 1990, 29, 434–438.

(79). Deacon GB; Phillips RJ Relationships between the carbon-oxygen stretching frequencies of carboxylato complexes and the type of carboxylate coordination, Coord. Chem. Rev 1980, 33, 227–250.

(80). Rehder D; Pessoa JC; Geraldes CFGC; Castro MMCA; Kabanos T; Kiss T; Meier B; Micera G; Pettersson L; Rangel M; Salifoglou A; Turel I; Wang D In vitro study of the insulin-mimetic behaviour of vanadium(IV, V) coordination compounds, J. Biol. Inorg. Chem 2002, 7, 384–396. [PubMed: 11941496]

(81). Velayutham M; Varghese B; Subramanian S Magneto-structural correlation studies of a ferromagnetically coupled dinuclear vanadium(IV) complex. Single-crystal EPR study, Inorg. Chem 1998, 37, 1336–1340. [PubMed: 11670342]

(82). Silverstein RM; Bassler GC; Morrill T Spectrometric Identification of Organic Compounds (5th Ed.). John Wiley & Sons, Inc.: Singapore, 1991; p 110–115.

(83). Strandberg GW; Wilson PW Formation of the nitrogen-fixing enzyme system in Azotobacter vinelandii, Can. J. Microbiol 1968, 14, 25–31. [PubMed: 5644401]

(84). Kim CH; Newton WE; Dean DR Role of the MoFe protein. α-subunit histidine-195 residue in FeMo-cofactor binding and nitrogenase catalysis, Biochemistry 1995, 34, 2798–2808. [PubMed: 7893691]

(85). Paustian TD; Shah VK; Roberts GP Apodinitrogenase: purification, association with a 20-kilodalton protein, and activation by the iron-molybdenum cofactor in the absence of dinitrogenase reductase, Biochemistry 1990, 29, 3515–3522. [PubMed: 2162195]

(86). Sheldrick GM A short history of SHELX, Acta Cryst 2008, A64, 112–122.

(87). Dolomanov OV; Bourhis LJ; Gildea RJ; Howard JAK; Puschmann H OLEX2: a complete structure solution, refinement and analysis program, J. Appl. Cryst 2009, 42, 339–341.

(88). Sheldrick GM Crystal structure refinement with SHELXL, Acta Cryst 2015, C71, 3–8.

(89). Frisch MJ, G. W. T., Schlegel HB, Scuseria GE, Robb MA, Cheeseman JR, Scalmani G, Barone V, Mennucci B, Petersson GA, Nakatsuji H, Caricato M, Li X, Hratchian HP, Izmaylov AF, Bloino J, Zheng G, Sonnenberg JL, Hada M, Ehara M, Toyota K, Fukuda R, Hasegawa J, Ishida M, Nakajima T, Honda Y, Kitao O, Nakai H, Vreven T, Montgomery JA Jr., Peralta JE, Ogliaro F, Bearpark M, Heyd JJ, Brothers E, Kudin KN, Staroverov VN, Kobayashi R, Normand J, Raghavachari K, Rendell A, Burant JC, Iyengar SS, Tomasi J, Cossi M, Rega N, Millam JM, Klene M, Knox JE, Cross JB, Bakken V, Adamo C, Jaramillo J, Gomperts R, Stratmann RE, Yazyev O, Austin AJ, Cammi R, Pomelli C, Ochterski JW, Martin RL, Morokuma K, Zakrzewski

VG, Voth GA, Salvador P, Dannenberg JJ, Dapprich S, Daniels AD, Farkas Ö, Foresman JB, Ortiz JV, Cioslowski J, Fox DJ Gaussian 09, Gaussian, Inc., Wallingford CT, 2009

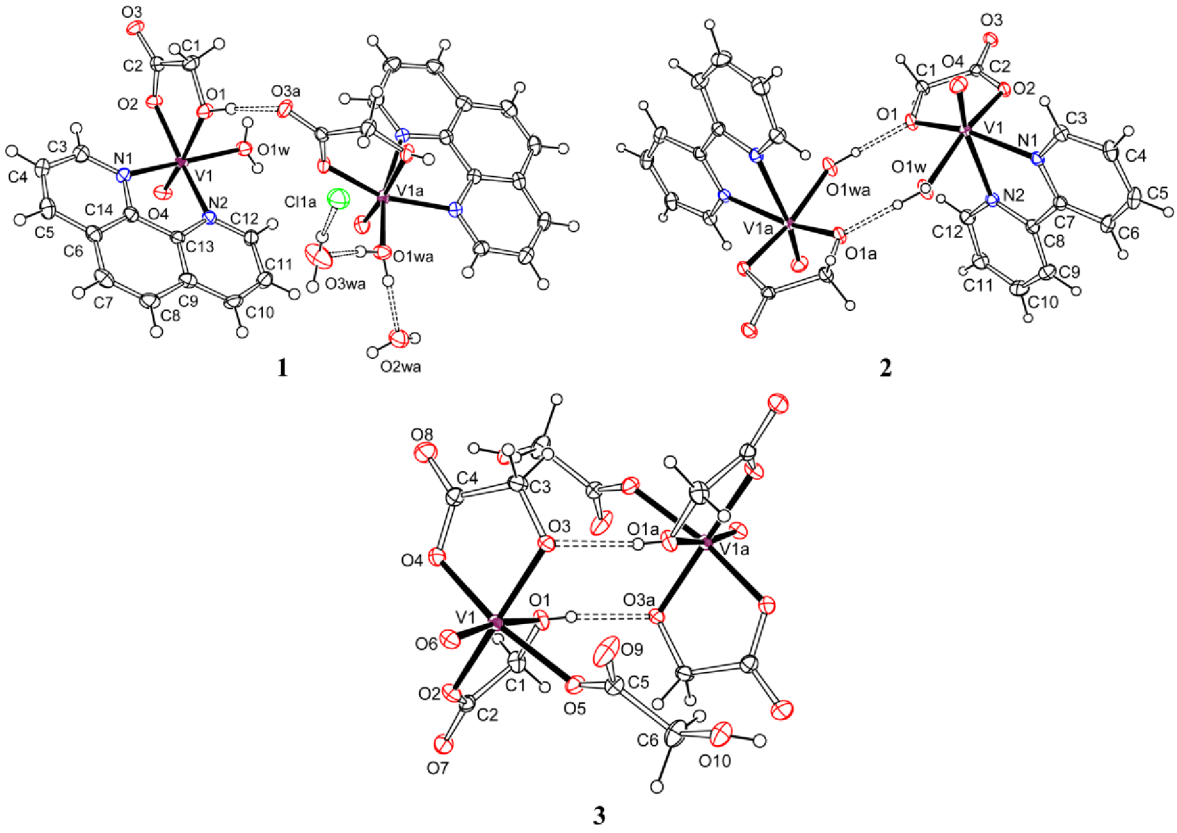

Figure 1.

The environment of $[VO(Hglyc)(phen)(H_2O)]Cl{\cdot}2H_2O$ (**1**) showing hydrogen bonds between α-hydroxy groups, water molecules and α-carboxy groups; $[VO(glyc)(bpy)(H_2O)]$ (**2**) showing hydrogen bonds between water molecules and α-alkoxy groups; $(NH_4)_2[VO(Hglyc)_2(glyc)]{\cdot}H_2O$ (**3**) showing hydrogen bonds between α-hydroxy groups and α-alkoxy groups. Ammonium ions and lattice water molecules were omitted for clarity.

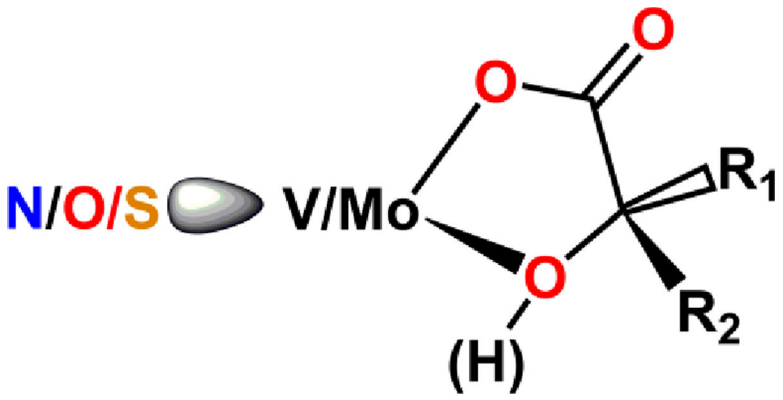

Figure 2.
The structures of model vanadium/molybdenum hydroxycarboxylates with low oxidation states.

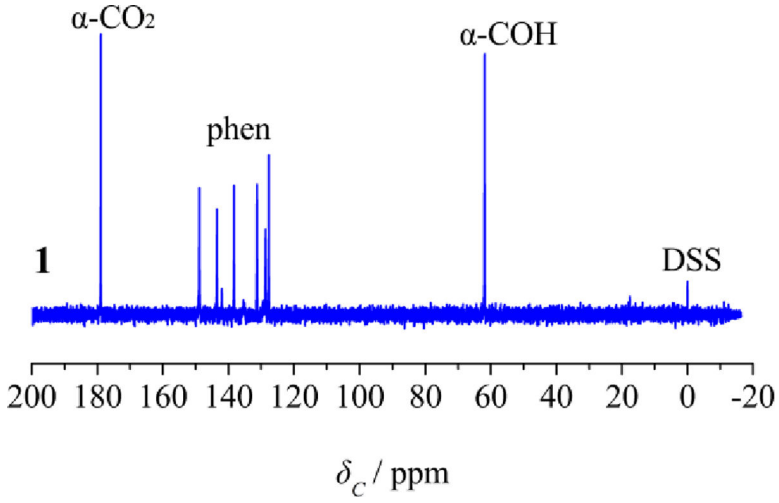

Figure 3.
Solution ^{13}C NMR spectrum of [VO(Hglyc)(phen)(H_2O)]Cl·2H_2O (**1**) in D_2O.

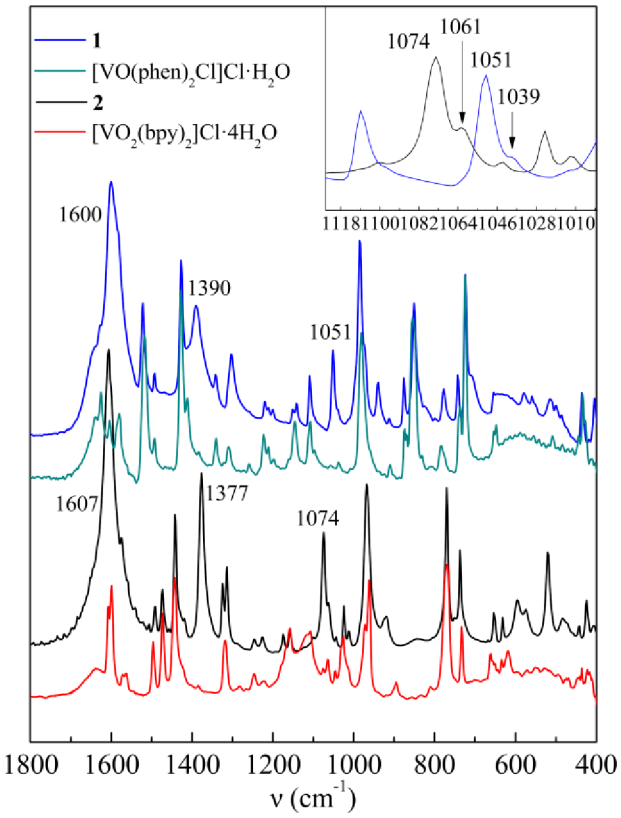

Figure 4.

FT-IR spectra of [VO(Hglyc)(phen)(H_2O)]Cl·2H_2O (**1**), [VO(phen)$_2$Cl]Cl·H_2O, [VO(glyc)(bpy)(H_2O)] (**2**) and [VO_2(bpy)$_2$]Cl·4H_2O in the regions of 1800–400 cm^{-1}.

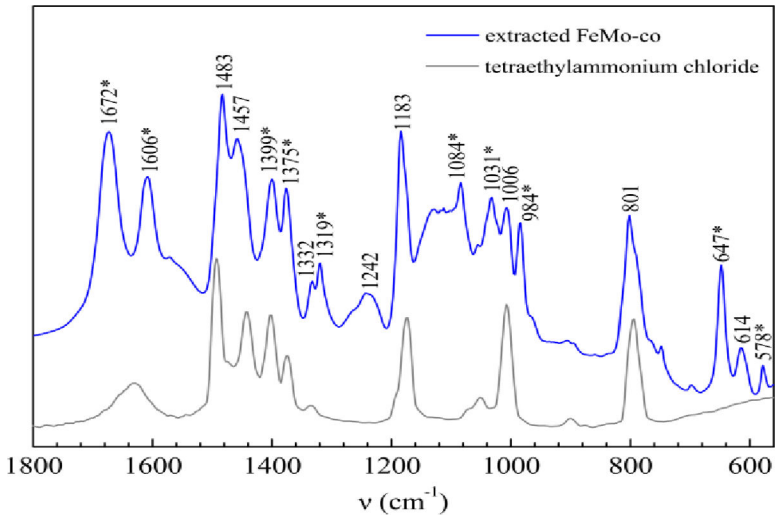

Figure 5.

FT-IR spectra of extracted FeMo-co and tetraethylammonium chloride (TEAC) in the region of 1800−560 cm^{-1}.

Table 1.

Comparisons of V/Mo–O bond distances (Å) in α-hydroxycarboxylato vanadium/molybdenum complexes.

Complexes	M–O (α-hydroxy)	M–O (α-alkoxy)	M–O (α-carboxy)
1	2.231(2)		1.997(2)
2		1.931(2)	2.018(2)
3	2.244(2)	1.927(2)	$2.027(2)_{av}$
$V^{IV}O$[34,64–66]	$2.210(5)_{av}$	$1.925(4)_{av}$	$2.010(5)_{av}$
$V^{IV}{}_2O_2$[38,39,43,44]		$2.020(5)_{av}$	$2.019(6)_{av}$
$V^{IV/V}{}_2O_3$[41]		$1.856(4)_{av}$	$2.080(4)_{av}$
$V^{V}{}_2O_4$[42,44–52,65]		$1.985(8)_{av}$	$1.975(8)_{av}$
FeV-co[1] (1.35 Å)	2.170_{av}		2.112_{av}
FeV-co[7] (1.2 Å)	2.160_{av}		2.104_{av}
Mo^0 (non-nature)[68]	$2.273(8)_{av}$		$2.233(8)_{av}$
Mo^{IV} [3,67]	$2.204(4)_{av}$	$2.010(3)_{av}$	$2.121(4)_{av}$
Mo^{V} [58,59,62,63]		$2.001(8)_{av}$	$2.142(12)_{av}$
Mo^{VI} [53–61]		$1.959(8)_{av}$	$2.203(7)_{av}$
FeMo-co[2](1.0 Å)	2.171_{av}		2.202_{av}

*The subscript *av* represents an average value. The detail data can be available in Tables S5 ~ S7 in Supplementary Information (SI†).

Table 2.

The C−O(H) bond distances (Å) and IR vibrational frequencies (cm^{-1}) of $C-O_{\alpha\text{-alkoxy}}$ or $C-O_{\alpha\text{-hydroxy}}$ groups.

Samples	C−O(H) distances (Å)	Frequencies (cm^{-1})
Protonated		
$[V^{IV}O(Hglyc)(phen)(H_2O)]Cl\cdot 2H_2O$ (**1**)	1.422(4)	1051.4m, 1039.5w
$[V^{IV}O(Hmal)(bpy)]\cdot H_2O$[34]	1.433(4)	1085.3m, 1030.5m
$[V^{IV}O(S\text{-}Hcitmal)(bpy)]\cdot 2H_2O$[34]	1.444(5)	1059.6w, 1035.5m
$[V^{IV}O(H_2cit)(bpy)]\cdot 2H_2O$[34]	1.440(8)	1068.7m, 1032.7s
$(Et_4N)_2[Mo^0(Hmal)(CO)_3]$[68] (non-nature)	1.440(5)	1007w
$(Et_4N)_3[Mo^0(Hcit)(CO)_3]$[68] (non-nature)	1.462(4)	1005m
$(Et_4N)_2[Mo^0(Hcitmal)(CO)_3]$[68] (non-nature)	1.44(1)	1007w
Deprotonated		
$[V^{IV}O(glyc)(bpy)(H_2O)]$ (**2**)	1.412(3)	1074.4s, 1061.0m
$K_2[Mo^{VI}O_2(glyc)_2]\cdot H_2O$[53]	$1.404(5)_{av}$	1094s, 1082s, 1066s
$[Mo_3SO_3(glyc)_2(im)_5]\cdot im\cdot H_2O$[3]	$1.408(3)_{av}$	1099.0m, 1070.9s
$\{Na_2[Mo^{VI}O_2(S\text{-}lact)_2]\}_3\cdot 13H_2O$[53]	1.427(8)	1085s, 1057s
$Na_2[Mo_3SO_3(R,S\text{-}lact)_3(im)_3]\cdot 10H_2O$[3]	$1.404(4)_{av}$	1095.4m, 1060.8m, 1049.9m
$[V^{IV/V}{}_2O_3(phen)_3(Hcit)_2(phen)_3O_3V_2]\cdot 12H_2O$[41]	1.410(2)	1073m
$(NH_4)_4[(Mo^{VI}O_3(cit)]\cdot 2H_2O$[57]	1.422(3)	1093m, 1073m
$[(Mo^{V}O)_2O(bpy)_2(H_2cit)_2]\cdot 4H_2O$[58]	$1.435(5)_{av}$	1078m
$[(Mo^{V}O_2)_2(phen)(H_2cit)(H_2O)_2]\cdot H_2O$[58]	1.419(8)	1086m
$[V^{IV/V}{}_2O_3(phen)_3$ (R,S-H_2homocit)$_2(H_2O)]Cl\cdot 6H_2O$[41]	1.410(7)	1084m
$K_2[Mo^{VI}O_2(R,S\text{-}H_2homocit)_2]\cdot 2H_2O$[61]	$1.419(2)_{av}$	1083.8m
Protonated and deprotonated		
$(NH_4)_2[V^{IV}O(Hglyc)_2(glyc)]\cdot H_2O$ (**3**)	$1.415(4)_{av}$	1088.3s, 1064.5s
$[Mo^{IV}{}_3S_4(PPh_3)_3(Hlact)_2lact]$[67]	$1.431(9)_{av}$	1090s, 1036s
FeV-co	1.443_{av}[1, 7]	---

Samples	C–O(H) distances (Å)	Frequencies (cm^{-1})
FeMo-co	1.449_{av}[3]	1084s, 1031s

Table 3.

Qualitative assignments of the most intensive bands in IR spectrum of extracted FeMo-co.

Frequency assignments (cm^{-1})			
Our work		**Orme-Johnson's work[9]**	
1672	$\nu_{as}(CO_2^-)$+ Partial NMF	1664	NMF
1606	$\nu_{as}(CO_2^-)$	1600	$\nu_{as}(CO_2)$
1483	TEAC		
1457	TEAC		
1399	$\nu_s(CO_2^-)$+ Partial TEAC	1389	$\nu_s(CO_2^-)$
1375		1357	$\nu_s(CO_2^-)$
1332	TEAC		
1319	-		
1242	NMF		
1183	ν(C–C)+ Partial TEAC	1127	dithionite
1084	ν(C–O)		
1031	ν(C–OH)		
1006	TEAC	1002	
984	-		
801	TEAC	842	
647	-		
614	NMF		
578	ν(Mo–O)		